



DETECTION OF ANIMAL OCCURRENCE USING AN UNMANNED SYSTEM*

J. Lešetický, P. Matějka, M. Olmr

Czech University of Life Sciences Prague, Faculty of Engineering, Prague, Czech Republic

In recent decades, there has been an increase in the work speed and breadth of agricultural technology used to mow grasses. This modernization has resulted in a decline in wildlife. There are several conventional ways to prevent these losses. The most well-known and simplest technique is to search for wild animals using dogs and a phalanx. The dogs are trained to systematically search the area and drive the animals out. Efficiency is increased when visiting a site regularly, thus disturbing the animals, which are then consequently less likely to fawn. The effectiveness of the swarm line depends on the number of participants involved. The recommended spacing is set at 1–3 m. An effective modern means seems to be the use of an unmanned system and thermal cameras. This article presents a proof of concept of a detection system that is capable of detecting the object searched for in grassy vegetation with more than 96% success, regardless of the flight level. The study contributes to automated detection based on the basic principles of threshold.

unmanned aerial vehicle, harvest, animal detection, animal monitoring, image analysis



doi: 10.2478/sab-2019-0028

Received for publication on November 6, 2018

Accepted for publication on April 10, 2019

INTRODUCTION

During agricultural operations, especially during haymaking, thousands of wild animals are injured or killed every year. The highest losses occur for roe deer (*Capreolus capreolus*) fawns. More specifically, in the Czech Republic, approximately 50 roes per 1000 ha are yearly killed by mowers (D i v i s o v a , 2015). In neighbouring Germany, the estimated death rate is about 500 000 wild animals a year in forage areas and grass meadows. Based on the annual increase in wild animals the estimates are: Sweden 25–44%, Poland 17–44% and Bulgaria 27% (C e r r a et al., 2009; S t e e n et al., 2012; W a g n e r , 2012).

The main causes include an increase in the area of permanent grassland and forage areas, which serve as a source of food and a natural shelter from predators for animals. When there is danger, young animals do not escape from the dangerous area, but instinctively find a hiding spot and wait for their parents to return (R i e c k , 1955). Technological advances in the performance of harvesting machines also have a major impact. From the viewpoint of agrotechnical deadlines, pressure on harvests in May and June increases, which very often coincides with the period when young animals are fawned. Harvest during this period is intended for livestock feeding and the operation of biogas stations. The killing of wild animals causes

* Supported by the Internal Grant Agency of the Czech University of Life Sciences Prague, Project No. 31170/1312/3122.

Table 1. Basic parameters of RGB camera and thermal camera

Size	RGB camera 20 × 13 × 6 mm	Thermal camera 445 × 254 × 254 mm
Mass	6 g	14.2 g
Spectrum/wavelength	Visible RGB	LWIR/(7.5 – 14) μm
Resolution	600 TVL	320 × 240 px
View angle	120°	32° × 24°
Temperature range	–	–40°C to 330°C

not only a reduction in their count, but also the risk of contamination of harvested feed for livestock which may cause botulism (Jarnemo, 2002).

Various methods of detecting wild animals based on infrared sensors (Moser, 2008; Wagner, 2012), microwave sensors (Petrovsky, Biebl, 2005; Fackelmeier, Biebl, 2009) or a thermal camera placed on the harvester (Steen et al., 2012) are currently available. All of these methods are susceptible to false detection due to vibration or inclination to the searched wild animals. For these reasons, it is appropriate to use modern unmanned vehicles (UAV) (Israel, 2012).

Today, drones are used in many areas such as in the forestry industry (reducing the number of fires) (Christensen, 2015; Tang, Shao, 2015) or as a diagnostic tool of photovoltaic farms (Avdelidis et al., 2011; Kauppinen et al., 2015), etc.

The combinations of thermal camera and unmanned vehicle (UAV) is also used for monitoring wild animals – e.g. sea turtles, black bears, large land mammals such as elephants (Bevan et al., 2015), wildlife (dos Santos et al., 2014), for fighting against poaching animals such as the rhinoceros (Muleropazmany et al., 2014), and for animals detection during agricultural processes (Israel, 2012; Felipe et al., 2016; Gonzalez et al., 2016). Machine learning is needed to automate the process of animal detection.

Christiansen et al. (2014) used an algorithm for their experiment, which is one of the nonparametric methods of classifying machine learning and covers also learning with a teacher. The principle of the algorithm is based on similarity with the nearest neighbours. The results published by Christiansen et al. (2014) show good detection and classification (accuracy 84.8%) up to 10 m. At a height of 10–20 m, the performance and accuracy of classification (75.2%) decrease. The proposed detection becomes unreliable at flight levels above 20–22 m, where classification accuracy is around or below 50% (Christiansen et al., 2014).

This article presents a low-cost system for searching for wild animals based on basic computer vision (Threshold).

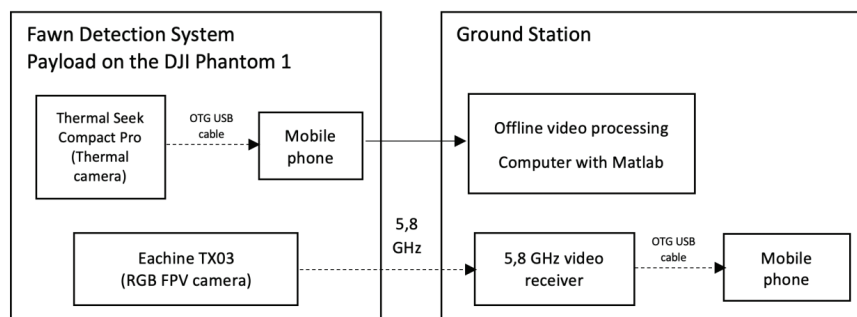
The aim of the research is to verify the feasibility of the detection system that will have an animal detection reliability of at least 95%, and the computationally-demanding data processing will not exceed the performance of a computer hung on a UAV and will be adaptable to the flight level. In the first stage of the development presented herein, a video is evaluated in the MATLAB environment after carrying out the aviation work.

MATERIAL AND METHODS

The tested search system prototype consists of two parts: detection and ground station. The detection part consists of a UAV (DJI Phantom 1 F300), two-axis stabilization units, Seek Thermal CompactPRO thermal cameras, and an Eachine TX03 RGB FPV camera. The basic parameters of both cameras are specified in Table 1.

The ground station consists of a mobile phone with OTG support and a video receiver (5.8G 32CH OTG FPV Receiver), where the visible spectrum Eachine TX03 camera (5.8 GHz) is displayed. Upon completion of the aviation work, the recorded video in the IR spectrum is downloaded to a computer where it is

Fig. 1. System architecture diagram



evaluated using the algorithm presented below created in the Matlab environment. Fig. 1 shows a simplified diagram of the architecture of the search system.

Testing of the search system was carried out at the beginning of July (July 6–7th, 2018) when haymaking peaked in Žlebské Chvalovice (49°53'23.5"N, 15°34'06.7"E) (Fig. 2a). The measurements were carried out at noon at temperatures 22.8–24.0°C and a wind force 8–10 m s⁻¹. It was cloudy on 6th July 2018 and half covered sky on 7th July 2018 (data provided by Čáslav meteorological station). For our study we used a dog – a warm-blooded animal, specifically, the Cavalier King Charles Spaniel (Fig. 2b) due to its size reminiscent of a freshly born roe calf.

As in the Czech Republic the use of UAVs for experimental and research purposes is subject to pilot and machine registration, it was necessary to anchor the UAV with the search system by means of a safety rope. In order to ensure the same position of the animal in the scanned area during measurement, the dog's leash was loaded with two bricks. The height of the stand ranged from 65 to 110 cm. The flight level of the machine was not constant and ranged from 5 to 20 m (average 9 m) and was measured using a laser rangefinder.

The recorded IR video was subsequently processed off-line in the MATLAB environment. In the proposed algorithm, the video is converted frame-by-frame. Each frame is first converted into a matrix in which each element acquires a value between 0–255. The value 0 represents the darkest pixels (black) and represents the lowest temperature of the image. In contrast, the 255 value represents the lightest pixels and represents the highest temperature. Specifically, the lowest temperatures (air temperatures 22.8–24.0°C) were achieved by grassland. In locations where there was direct visibility of the soil, a maximum temperature of 33°C was measured. The searched object (dog)

reached a maximum surface temperature of 50°C and was therefore interpreted by the brightest pixels (value of 255). Just like humans, warm-blooded animals try to maintain a constant body temperature ($\epsilon > 0.95$). In particular the coat of fresh-born baby has a low insulating ability and is visible in the infrared spectrum (Gade, Moeslund, 2014). On this basis, pixels are the subject of interest in the created matrix, which will gain intensity values from 127.5 to 255. The approximated 3D histogram (depiction of each 8th pixel) of the original image matrix is shown in Fig. 3a). The imadjust function is used to obtain the pixels that can be the searched object. The imadjust function works on the principle of the 'to zero' thresholded type (OpenCV team, 2018):

$$dst(x,y) = \begin{cases} src(x,y)-thresh & \text{if } src(x,y) > thresh \\ 0 & \text{otherwise} \end{cases} \quad (1)$$

where:

x, y = pixel coordinates

$thresh$ = set threshold

If the current $src(x,y)$ pixel value is lower than the set $thresh$ value, the new pixel value is set to 0 (black). If the current $src(x,y)$ pixel value is higher than the determined $thresh$ value, the $thresh$ value will be subtracted from the current $src(x,y)$ value. The approximate 3D view of the modified image matrix of the imadjust function is shown in Fig. 3b).

An adaptive threshold (the adaptthresh function) is applied to a newly created image, and it uses the Gaussian weighted average of pixel intensities in the neighbourhood to calculate the local threshold for each pixel. The basis for calculating the adaptive threshold level is the 'Gaussian blur' (2).

$$g(x,y) = \frac{1}{\sqrt{2\pi\sigma}} \left(-\frac{x^2+y^2}{2\sigma^2} \right) \quad (2)$$



Fig. 2a. Images from the Measurement Area



Fig. 2b. Images from the Measurement Area

where:

x^2, y^2 = size of the filtration mask (*filterSize*)

σ = blur parameter

The size of the filtration mask (*filterSize*) is expressed as:

$$filterSize = 2 \left\lfloor \frac{sizeIMG}{16} \right\rfloor + 1 \quad (3)$$

In this study, the size of the filtration mask *filterSize* ($x^2 = 161, y^2 = 91$) was calculated by formula (3), which is part of the *adaptthresh* function. The image size (*sizeIMG*) was 1280 × 720 px. The blur parameter (σ) was left at a base value of 0.5, which was also used in the study (Steen et al., 2012). The threshold level (*T*) is determined according to:

$$T = scaleFactor \cdot g(x,y) \quad (4)$$

The value of the variable (*scaleFactor*) for the image was set at the highest sensitivity (1.5). The

threshold values (*T*) of each pixel are depicted in an approximate 3D view (Fig. 4a). The calculated *T* is transferred to the function (*imbinarize*), which is equivalent to the binary Threshold (5) (OpenCV dev team, 2018):

$$dst(x,y) = \begin{cases} maxVal & \text{if } src(x,y) > thresh \\ 0 & \text{otherwise} \end{cases} \quad (5)$$

If the value of the current pixel *src(x,y)* is greater than the set value *thresh*, this pixel is set to *maxVal* – maximum value (255 – white). The other values *otherwise* are set to a 0 value (black). The approximate 3D view is shown in Fig. 4b.

Regions and their sizes are counted in the newly created image. If the size of the area is less than 100 px or greater than 14 000 px, then they are removed. The goal of the proposed algorithm is the ability to detect an object (in this study the dog) in the video. In Fig. 4b it can be seen that the searched object has the warmest (brightest) body and head section, which

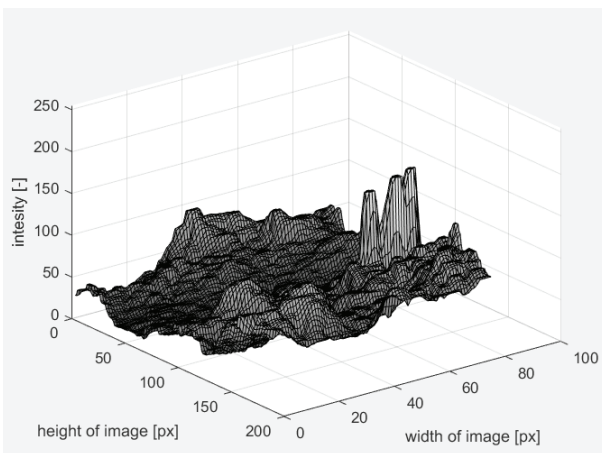


Fig. 3a. 3D representation original image

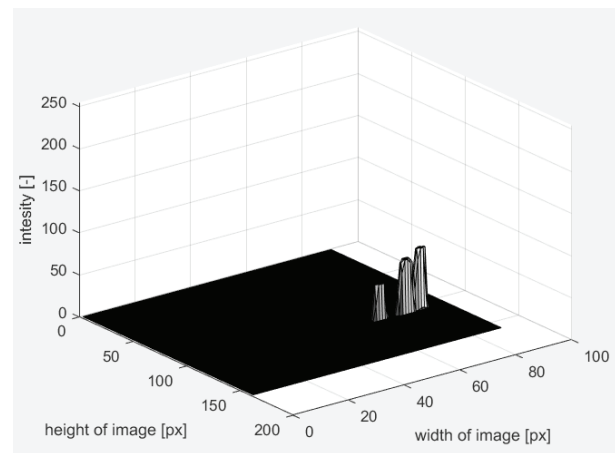


Fig. 3b. 3D representation image after *imadjust* function

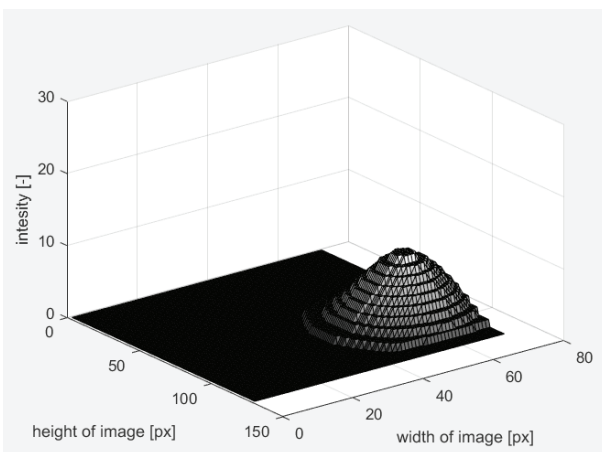


Fig. 4a. 3D representation of *T* variable

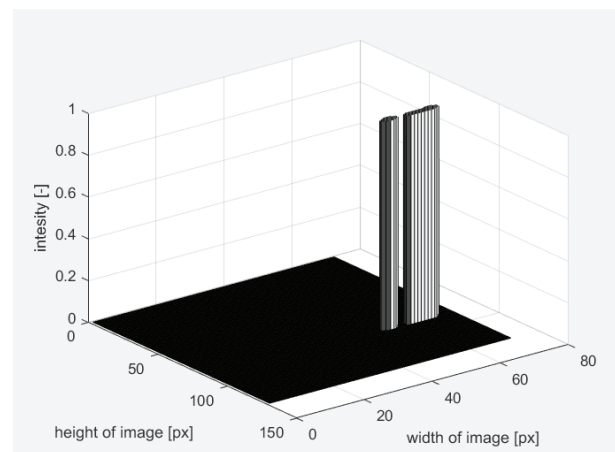


Fig. 4b. 3D representation - frame after *adaptthresh* function

is divided into two regions. Morphological functions (dilation and erosion) are carried out to ensure that the searched objects are properly evaluated, specifically, when detecting two regions of 100 px, three regions of 75 px, four regions of 50 px, and five regions of 25 px. Edge detection (Canny) is then carried out. The highlighted edges are entered back into the original image and the searched objects are thereby highlighted. The output of the algorithm are images in five detected regions and a video containing information (image number, number of objects, size of objects) for retroactive evaluation of the proposed algorithm. Fig. 5 shows the processing of the image using the proposed algorithm in steps: (a) original frame, (b) frame after imadjust function, (c) frame after adaptthresh function, (d) frame after edge detection.

RESULTS

The overall detection reliability is dependent on the imadjust function level that separates the foreground of the image, which is the subject of interest, from the background. In order to determine the optimum level value, a level from 0.5~127.5 intensity to 0.8~204 intensity step by step from 0.01~2.62 brightness intensity was set for all of the images (3101 images). Overall, 51 563 images were evaluated, which were divided firstly according to the number of objects (1–5) and then depending on whether or not the searched object is in the image. The results were recorded and processed in Excel, where the correlation coefficient dependencies of individual evaluated objects (positive detection and false positive detection) on the thresh-

Table 2. Correlation coefficients

	Object	Threshold level
Positive detection	No. 1	0.3318
	No. 2	-0.0029
	No. 3	-0.8905
	No. 4	-0.8067
	No. 5	-0.7147
	total positive	0.7256
False positive detection	No. 1	0.9435
	No. 2	0.9756
	No. 3	0.9613
	No. 4	0.9491
	No. 5	0.9191
	total false positive	0.9874

old level were evaluated. The correlation coefficients (Table 2) show that for positive detection the dependence is strong but indirect in the case of detection of three, four and five objects (-0.89; -0.8; -0.7). For the detection of 1 and two objects (0.331; -0.002), it can be stated that there is almost no dependency. The total number of positives and false positives of the detected images shows a strong and direct dependence (0.725; 0.987) on the threshold level. The number of images evaluated as false positives in all cases has a growing tendency with the value of the set threshold level (Fig. 6).

The measurement results are plotted into graph (Fig. 7) according to the number of detected objects,

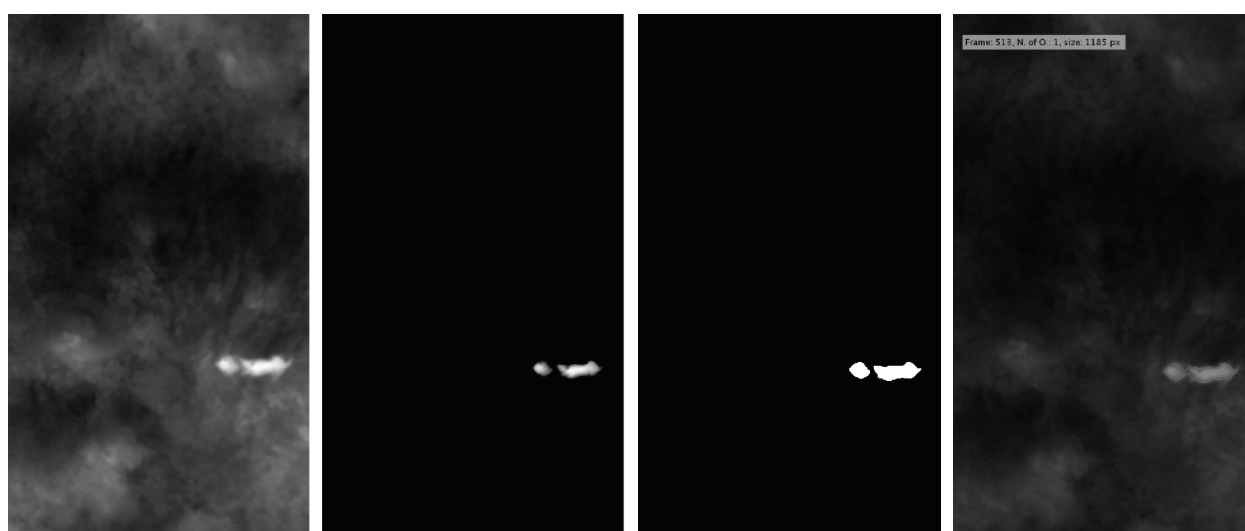


Fig. 5a. Image processing - Original frame

Fig. 5b. Image processing - Frame after imadjust funkcjon

Fig. 5c. Image processing - Frame after adptthresh funkcjon,

Fig. 5d. Image processing - Frame after edge detection (final frame).

total positive detection and false positive detection. In order to determine the optimal threshold level, the area in which it should be located is first defined using the following conditions: the minimum unrecognized image values (3.54%) are achieved at a threshold level of 0.64 (~163.2 brightness intensity) and thereby also maximum detection reliability (96.4%). The minimum values (13.3%) of total false positive images are achieved at a level of 0.62 (~158.1 brightness intensity). These conditions were obtained at the interval ($< 0.62; 0.64 >$).

The specific threshold value of the found interval is dependent on the algorithm's application, i.e. the extent to which false positive results are undesirable. The recommended value for threshold setting is the level of 0.63, at which the algorithm has 96.2% success rate for finding the object if the object is actually in the image, and 13.9% false positive detection if the object is not in the image. It can be seen from this graph that an error rate in the algorithm may occur

in terms of the number of detected objects in the image, specifically for one and two objects. This error is caused by the creation of two regions (the head and the torso), on which there is more sunlight than on the animal's neck. This error rate can be suppressed by changing the coefficients of morphological functions.

DISCUSSION

The goal of this proof concept was to create an algorithm that will be able to detect animals with at least 95% success regardless of the number of detected objects and the flight level. The achieved success rate of detection was even higher than the success rate published in Christiansen et al. 2014, referring to 84.8% under a 10 m flight level. In real conditions, there will be a situation where more animals are assigned to one object via detection. Typically, this can happen in situations where more animals squeeze each

Fig. 6. Graph of false positive detection frames

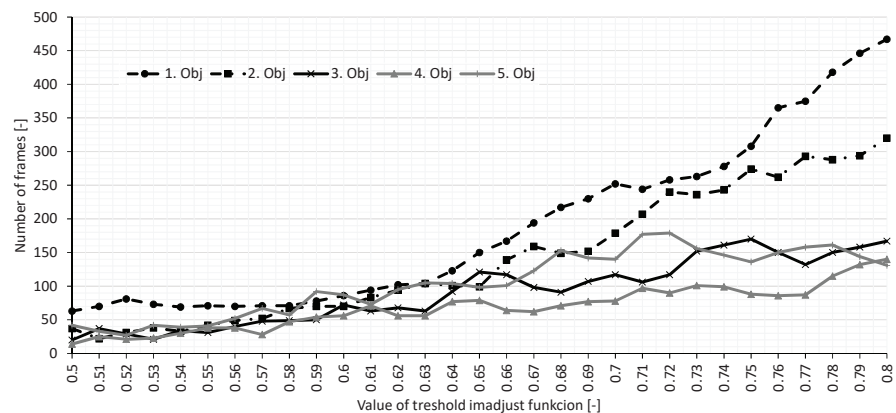
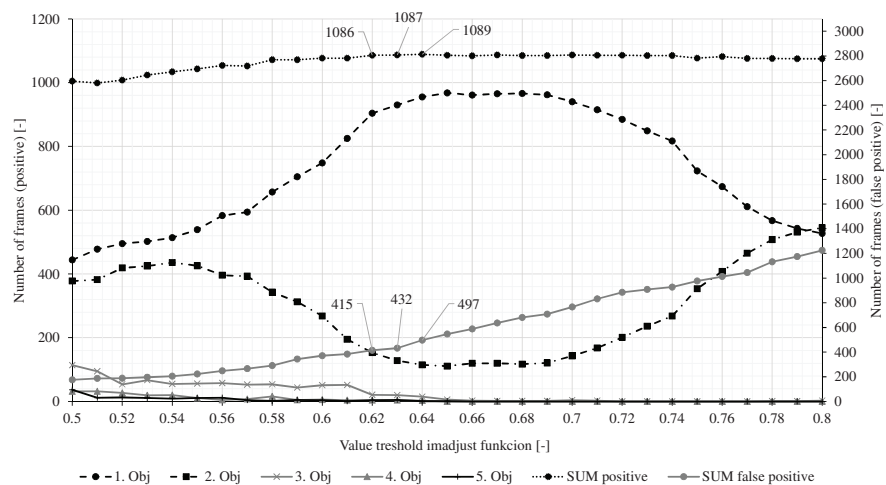


Fig. 7. Error rate of detection frames



other in one pack. However, this property is not a major obstacle in using the system because the number of animals in the pack does not matter in this case.

While testing the proposed detection system, it was found that hardware performance and the Android operating system are the right way to improve it. The subsequent part of the research considers the use of the full potential of a mobile phone for which an application will be created that will use the presented algorithm and will be expanded by GPS coordinates in the event of positive detection. These coordinates will be sent to the ground station along with approximately 5-second IR video recording of the scanned scene.

CONCLUSION

A total of 3101 images were taken in the study in which the object searched for (dog) was found in 1129 images. The images were exposed to thirty threshold levels (0.5–0.8) corresponding to values of 127.5–204 brightness intensity. At each step, the threshold level was increased by 0.01 (~2.62 brightness intensity). The highest success of the proposed algorithm was achieved at the threshold level of the imadjust function (0.63~160 brightness intensity). At this level, 1087 out of 1129 images with the dog were detected and its success rate is therefore 96.2%. The number of objects was evaluated from the positively evaluated images, where 85.5% of the images were evaluated as one object, 11.7% of the images as two objects, 1.84% of the images as three objects and 0.83% as four or five objects. These results can be improved via a higher morphological function (dilation and erosion) that is tied to the number of searched objects. Increasing cutting levels (threshold) also increased false positive images, of which 14% were evaluated from the total 3101 images. The number of these images can be reduced in the part of the algorithm in which the values are set for deleting miniature and large objects that cannot be the searched object. Therefore, in the next phase of our research, a direct connection of an unmanned aircraft to the algorithm will be tested.

REFERENCES

Avdelidis NP, Markopoulos YP, Katsis IA, Kouli M (2011): A thermographic survey for evaluating *in situ* the performance of photovoltaic panels In: Proc. SPIE 8013: Thermosense: Thermal Infrared Applications XXXIII. Orlando, USA, Article No. 80130K. doi: 10.1117/12.883367.

Bevan E, Wibbels T, Najera BMZ, Martinez MAC, Martinez LAS (2015): Unmanned aerial vehicles (UAVs) for monitoring sea turtles in near-shore waters. *Marine Turtle Newsletter*, 145, 19–22.

Cerra D, Israeland M, Datcu M (2009): Parameter-free clustering: Application to fawns detection. In: Proc. Internat.

Geoscience and Remote Sensing Symposium, Cape Town, South Africa, III467–III469.

In Geoscience and Remote Sensing Symposium, 2009 IEEE International, IGARSS 2009, volume 3, pages III–467. IEEE, 2009.

Christensen BR (2015): Use of UAV or remotely piloted aircraft and forward-looking infrared in forest, rural and wildland fire management: Evaluation using simple economic analysis. *New Zealand Journal of Forestry Science*, 45, 16. doi: 10.1186/s40490-015-0044-9.

Christiansen P, Steen KA, Jorgensen RN, Karstoft H (2014): Automated detection and recognition of wildlife using thermal cameras. *Sensors (Switzerland)*, 14, 13778–13793. doi: 10.3390/s140813778.

Divisova M (2015): Project Save the Roe Deer Fawn. *Myslivořt*, 2015, 8, 36. <http://www.myslivořt.cz/Casopis-Myslivořt/Myslivořt/2015/Srpen-2015/Projekt-Zachranme-srncata>. Accessed 11 May, 2018. (in Czech)

dos Santos GAM, Barnes Z, Lo E, Ritoper B, Nishizaki L, Tejada X, Ke A, Lin H, Schurgers C, Lin A, Kastner R (2015): Small unmanned aerial vehicle system for wildlife radio collar tracking. In: Proc. 11th IEEE Internat. Conf. Mobile Ad Hoc and Sensor Systems (MASS), Philadelphia, USA, 761–766. doi: 10.1109/MASS.2014.48.

Fackelmeier A, Biebl EM (2009): A multistatic radar array for detecting wild animals during pasture mowing. In: Proc. 6th European Radar Conference EURAD 2009, Rome, Italy, 477–480.

Felipe L, Ward S, Gonzalez LF (2016): Autonomous UAVs wildlife detection using thermal imaging, predictive navigation and computer vision. In: IEEE Aerospace Conference, Big Sky, USA, 1–8. doi: 10.1109/AERO.2016.7500671.

Gade R, Moeslund TB (2014): Thermal cameras and applications: A survey. *Machine Vision and Applications*, 25, 245–262. doi: 10.1007/s00138-013-0570-5.

Gonzalez LF, Montes GA, Puig E, Johnson S, Mengersen K, Gaston KJ (2016): Unmanned aerial vehicles (UAVs) and artificial intelligence revolutionizing wildlife monitoring and conservation. *Sensors (Switzerland)*, 16, 97. doi: 10.3390/s16010097.

Israel M (2012): A UAV-based roe deer fawn detection system. *ISPRS – International Archives of the Photogrammetry, Remote Sensing and Spatial Information Sciences*, XXXVIII-1/C22, 51–55. doi: 10.5194/isprsarchives-XXXVIII-1-C22-51-2011.

Jarnemo A (2002): Roe deer *Capreolus capreolus* fawns and mowing – mortality rates and countermeasures. *Wildlife Biology*, 8, 211–218. doi: 10.2981/wlb.2002.035.

Kauppinen T, Panouillot PE, Siikanen S, Athanasakou E, Baltas P, Nikopoulos B (2015): About infrared scanning of photovoltaic solar plant. In: Proc. SPIE 9485: Thermosense: Thermal Infrared Applications XXXVII. Baltimore, USA, Article No. 948517.

Moser E (2008): i.s.a. – Infrared wildlife rescue 10 years in use – A field report. *OÖ Jäger*, 2008, 1. <http://www.wildretter.de/>

- fileadmin/user_upload/pdf/Der-Ooe-Jaeger-118-2008_Wildretter_10_Jahre_Erfahrung.pdf. Accessed 21 May, 2018. (in German)
- Mulero-Pazmany M, Stolper R, Van Essen LD, Negro JJ, Sassen T (2014): Remotely piloted aircraft systems as a rhinoceros anti-poaching tool in Africa. PLoS ONE, 9, e83873. doi: 10.1371/journal.pone.0083873.
- OpenCV dev team (2018): Basic thresholding operations. <https://docs.opencv.org/2.4/doc/tutorials/imgproc/threshold/threshold.html>. Accessed 21 June, 2018.
- Patrovsky A, Biebl EM (2005): Microwave sensors for detection of wild animals during pasture mowing. Advances in Radio Science, 3, 211–217. doi: 10.5194/ars-3-211-2005.
- Rieck W (1955): The setting time for roe deer, red deer and fallow deer in Central Europe. Zeitschrift für Jagdwissenschaft, 1, 69–75. doi: 10.1007/BF01907251.
- Steen KA, Villa-Henriksen A, Therkildsen OR, Green O (2012): Automatic detection of animals in mowing operations using thermal cameras. Sensors (Switzerland), 12, 7587–7597. doi: 10.3390/s120607587.
- Tang L, Shao G (2015): Drone remote sensing for forestry research and practices. Journal of Forestry Research, 26, 791–797. doi: 10.1007/s11676-015-0088-y.
- Wagner J (2012): From traditional methods of the rescue of the wild to modern techniques of the ‘savior of the wild’, 10, 32. <https://lars-wildretter.de/wp-content/uploads/2016/06/Johann-Wagner-Schach-dem-Maethod-2012.pdf>. Accessed 21 June, 2018. (in German)

Corresponding Author:

Ing. Pavel Matejka, Czech University of Life Sciences Prague, Faculty of Engineering, Department of Technological Equipment of Buildings, Kamýcká 129, 165 00 Prague 6-Suchbát, Czech Republic, phone: +420 224 383 223, e-mail: matejkapavel@tf.czu.cz
